Desalination and Water Treatment
www.deswater.com
doi: 10.5004/dwt.2021.27585

234 (2021) 77–90
September

Phosphate removal from water using activated carbon derived from *Ampelodesmos mauritanicus* stems: equilibrium and kinetic studies

A. Benhathat, M. Amrani*

Laboratory of Soft Technology, Recovering, and Sustainable Development, Faculty of Science, M'Hamed Bougara University of Boumerdes, Adependance Avenue, 35000, Algeria, Tel. +213-0560082355; email: moussaamrani@yahoo.fr (M. Amrani), Tel. +213-0699243996; email: amalbenhathat@hotmail.com (A. Benhathat)

Received 9 March 2021; Accepted 13 June 2021

ABSTRACT

This paper describes the synthesis and characterization of *Ampelodesmos mauritanicus* stem-derived activated carbon (AMSAC). The activated carbon was produced by phosphoric acid activation followed by carbonisation and was characterized by N_2 adsorption–desorption isotherm, scanning electron microscopy, energy-dispersive X-ray analysis, and Fourier-transform infrared (FTIR) spectroscopy. The sorption potential of AMSAC for the removal of phosphate ions from the water was investigated. The effects of contact time, initial pH, and initial phosphate concentration on the sorption process were studied. The optimum contact time and pH for removal of phosphate ions was 75 min and pH 6–7. The experimental data showed that AMSAC had a high Brunauer–Emmett–Teller surface area of 1,293 m^2/g and abundant pores with a specific volume of 1.23 m^3/g. FTIR analysis revealed various functional groups on the surface of the AMSAC, which can play an important role in the adsorption process. A Langmuir isotherm model fits the equilibrium data for the sorbent well compared to the Freundlich, Temkin, and Dubinin–Radushkevich isotherm models. The monolayer sorption capacity of AMSAC for PO_4^{-3} ions was determined to be 4.52 mg/g at 25°C. The experimental data were also modelled using the sorption kinetic models. It was found that the kinetic data were described better by the pseudo-second-order adsorption kinetic model. Therefore, AMSAC is a promising low-cost phosphate sorbent that can be produced from plentiful and annually renewable plants.

Keywords: Phosphoric acid; Adsorption isotherm; Phosphate; Characterisation; *Ampelodesmos mauritanicus*

1. Introduction

Phosphate discharged into water bodies such as lakes, ponds, and rivers are not considered toxic, but is responsible for eutrophication, which causes oxygen depletion, toxic algae blooms, and degradation of water quality [1,2]. Phosphate comes to water resources from agricultural fertilizers, detergents, erosion of soils, and discharge from sewage treatment plants and often presents in water and wastewater at various concentrations. The principal phosphorus compounds in wastewater are generally orthophosphates together with smaller amounts of organic phosphate [3]. Studies indicate that 10–15 mg/L phosphate may be contained in municipal wastewater, whereas effluent from chemical industries, such as detergent manufacturing and metal coating processes, may contain 14–25 mg/L phosphate [4,5]. Protection of water resources is an urgent task for healthy living and sustainable development. In many countries, stringent regulations limit phosphorous levels to 0.05 mg/L to maintain an ecologically sustainable status [6]. For water conservation, the removal of phosphates from waters and wastewaters to control eutrophication is of great importance. Phosphate removal from wastewater has been widely investigated, and several techniques have

* Corresponding author.

been developed, including physical processes (settling, filtration), chemical precipitation (with aluminium, iron, and calcium salts), and biological processes that rely on biomass growth (bacteria, algae, and plants) or intracellular bacterial polyphosphate accumulation [7–9]. The sorption process is generally considered to be an effective water treatment option to remove anions because of convenience, ease of operation, and simplicity of design and economics, provided that low-cost sorbents are used [10]. Recently, the adsorption of phosphate onto activated carbon derived from plant materials has received increasing attention, as activated carbon could be a low-cost and effective adsorbent for phosphate removal in water and wastewater [11,12].

The activated carbon that was investigated in this study was produced from the stems of the *Ampelodesmos mauritanicus* plant, which is a grass plant of the family Gramineae largely present in the Mediterranean area and, in particular, North Africa. It grows both in wet and dry areas and is abundantly available throughout the year, which makes it important biomass. The average height of the *A. mauritanicus* plant can exceed one meter, and their fibres are extremely sturdy and rough [13–15]. The main constituents of *A. mauritanicus* according to their weight proportions are cellulose (44.1%), hemicelluloses (27%), lignin (16.80%), extractives (9%), and ashes (3.1%) [16].

The aim of this work is to prepare activated carbon powder from *A. mauritanicus* stems using chemical activation with H_3PO_4 followed by carbonization in nitrogen atmosphere. Characterisation of the activated carbon obtained in the optimal conditions was conducted using the following techniques: Fourier-transform infrared (FT-IR) spectroscopy to determine the functional groups, Brunauer–Emmett–Teller (BET) method to determine surface area and average pore size, scanning electron microscopy (SEM) to investigate the structure and morphology, and iodine and methylene blue number. The potential of the prepared AMSAC is evaluated in the adsorption of phosphate ions (PO_4^{3-}) from water using batch experiments at different operating conditions namely the pH, the contact time, and the initial adsorbent concentration. Equilibrium and kinetic studies were also performed. The activation parameters calculated from the adsorption measurements in this study are very useful in elucidating the nature of adsorption.

2. Experimental

2.1. Sample preparation

2.1.1. Raw material

A. mauritanicus (Fig. 1) was collected from the northeast of the Boumerdes area, Algeria. This biomass material was harvested in early June 2016. The sample was washed with water to remove dirt, dried at 60°C for 8 h in an air oven, and reduced to about 2 cm in length with a razor blade for effective milling to a size less than 500 μm. The residues after this milling were used for the compositional analysis and production of AMSAC.

2.1.2. Adsorbent synthesis

A. mauritanicus strunk powder was thoroughly mixed with ortho-phosphoric acid H_3PO_4 solutions (85%) in a weight ratio of 1:2 g/g (ortho-phosphoric acid was purchased from Merck Germany) at room temperature for 1 h and then dried in an oven (Memmert UNB 400) at 105°C for 24 h. After the impregnation step, the sample was carbonized in a horizontal tube furnace (Nabertherm, Germany) under nitrogen atmosphere. The heating rate and the nitrogen flow rate were 5°C/min and 200 mL/min, respectively. The samples were kept at 500°C for 2 h. The crucibles were left inside the furnace for 24 h to cool down at room temperature. The prepared AMSAC samples were soaked in 0.1 N NaOH for 2 h, as the pH of the washing water reached about 5, and then with 2 L of hot de-ionized water under reflux until the pH of the rinsing water was neutral. The samples were filtered through a Whatman filter paper (0.45 μm) to separate the supernatant and the AMSAC particles. After that, it was dried in a hot air oven for 24 h, weighed, and packed in sealable plastic bags for further use.

2.1.3. Adsorbate

The 500 mg/L phosphate (PO_4^{3-}) stock solution was prepared by dissolving potassium dihydrogen orthophosphate (KH_2PO_4) powders (analytical reagent grade) in deionized water. Phosphate working solutions with different concentrations were prepared by diluting the PO_4^{3-} stock solution with distilled water and using 0.01 M KCl to adjust ionic strength. The pH value of the PO_4^{3-} working solution was adjusted with diluted HCl and NaOH before the adsorption experiments.

2.1.4. Adsorbent characterisation

The surface structure of AMSAC was investigated with a SEM, N_2 adsorption–desorption technique (BET method), FTIR, and X-ray diffraction (XRD). A SEM was used to characterize the nanoparticle shape and size using an FEI Quanta 650 scanner with an accelerating current of 80 μA and a voltage of 30 kV. SEM images were formed using transmitted electrons (instead of the visible light), which can produce magnifications up to 100.000 X with resolutions up to 100 Å. The BET surface area was measured by the N_2 adsorption–desorption technique using a Quanta Chrome Instruments Nova 2000 E analyzer. The total pore volume was defined as the volume of liquid

Fig. 1. Tuft of *Ampelodesmos mauritanicus*.

nitrogen corresponding to the amount adsorbed at a relative pressure of P/P_0 = 0.99. The mesoporous surface area and microporous volume were estimated using a *t*-plot [17]. The FTIR spectroscopy of the AMSAC was measured by an FTIR spectrometer Shimadzu 8400S from 4,000 to 400 cm^{-1}. The measurement was carried out with the KBr pellet method (0.5% of the sample in KBr). The crystalline structure was analyzed by the XRD using Cu-Kα radiation (1.5418 Å) of a Bruker D8 Advance diffractometer operating at 40 kV, 40 mA for angles between 2θ = 4°–90° in 0.02° steps. The bulk density was determined according to a procedure followed by Toshiguki and Yukata [18]. Moisture content was determined using an oven drying method [19]. Ash content was determined by a standard method [20]. The adsorption properties of the activated carbons where characterized in terms of both iodine adsorption and methylene blue adsorption indexes according to the procedure reported in the literature [21,22]. The phosphate content in the filtrates and initial solutions was measured by the molybdate blue complex spectrophotometric method at λ_{max} of 880 nm using a Lambda 25 UV/VIS spectrophotometer (Perkin-Elmer, Germany). This experiment was performed in triplicate and average values were reported.

2.3. Batch adsorption studies

2.3.1. Removal efficiency and adsorption capacity

The removal of phosphate ions from the aqueous synthetic solution was conducted using batch experiments, including isotherm studies, kinetic studies, and initial pH studies. All the experiments were conducted in batch mode by adding 50 mL of phosphate solution to 0.1 g of AMSAC (initial solution concentration ranging from 5 to 60 mg/L, temperature at 25°C ± 1°C, and pH = 6.8) in 250 mL Erlenmeyer flasks. The flasks were shaken using a horizontal shaker (Edmund Buhler 7400 Tubingen, SM 25, Germany) operating at 200 rpm for 50 min. After the shaking of the slurries, the suspensions were centrifuged using a centrifuge apparatus (HERAEUS MULTIFUGE 3RS, Kendro GmbH, Germany) operating at 3,000 rpm for 10 min and immediately filtered using a vacuum filtration pump employing a 0.45 μm filter to obtain a clear supernatant aliquot. The supernatant solution obtained from filtration was used for the phosphate analysis. The adsorbed and % removal of phosphate was computed using Eqs. (1) and (2), as indicated below:

$$q_e = \frac{\left(C_0 - C_t\right)V}{M} \tag{1}$$

$$\left(\%\right) = \frac{\left(C_0 - C_t\right)}{C_0} \times 100 \tag{2}$$

where q_t is the amount of phosphate adsorbed per unit mass of adsorbent (mg/g) at time *t*, C_0 and C_t are the initial and final concentration of phosphate at time *t* (mg/L), respectively, *V* is the volume of the solution contacted with the adsorbent (L), *M* is the mass of the adsorbent (g), and (%) is the percent removal at the time (*t*).

2.3.2. Effects of initial pH

For the initial pH studies, it was adjusted to be in the interval 2.0–14 with 0.1 N HCl or 0.1 N NaOH solutions using a pH meter (HANNA instruments pH 213). Experiments were conducted at an initial phosphate ion concentration of 40 mg/L, an adsorbent dose of 4 g/L, room temperature (25°C ± 1°C), and a spin time of 50 min.

2.3.3. Kinetic studies

For the kinetic study, AMSAC (0.2 g) was agitated for a selected time interval of 5, 10, 15, 30, 40, 80, 120, 160, and 200 min at 200 rpm in a series of 250 mL conical flasks containing 50 mL of aqueous solution (40 mg/L) of PO_4^{-3} and distilled water maintained at 25°C ± 1°C in the horizontal shaker. Each time interval was repeated three times to find the deviation in the measured value. In this work, the kinetic data were analyzed using the pseudo-first-order, pseudo-second-order, Elevich, and intra-particle-diffusion kinetic models with a calculation of the nonlinear chi-square test (Eq. (3)) of the adsorption capacity from each model. All the models used were linearized, and the model with a linearity closest to 1 with a lower percentage of variance was considered as the best model to explain the mechanism.

$$\chi^2 = \sum \frac{\left(q_{max} - q_{cal}\right)^2}{q_{max}} \tag{3}$$

where q_{max} and q_{cal} are the maximum and calculated amount of phosphate adsorbed (mg/g), respectively.

The equation for the pseudo-first-order kinetic model can be expressed by Eq. (4):

$$\log\left(q_e - q_t\right) = \log q_e - K_1 \frac{t}{2.303} \tag{4}$$

where K_1 is the rate constant of the pseudo-first-order model of adsorption (min^{-1}), and q_e and q_t are the amount of phosphate adsorbed (mg/g) at equilibrium and at time (*t*), respectively.

The values of K_1 and q_e can be obtained from the slope and the intercept of a linear straight-line plot of $\log(q_e - q_t)$ vs. *t*.

The equation for the pseudo-second-order kinetic model can be written as shown in Eq. (5):

$$\frac{t}{q_t} = \left(\frac{1}{K_2 q_e^2}\right) + \left(\frac{1}{q_e}\right)t \tag{5}$$

where K_2 is the rate constant of the pseudo-second-order model of adsorption (g/mg min). The value of K_2 and q_e can be obtained from the slope and intercept of a plot of t/q_t vs. *t* (min).

The Elovich equation was used to interpret the kinetics of sorption that was previously described as chemical sorption on highly heterogeneous sorbents. The equation had been simplified and linearized as shown in Eq. (6):

$$q_t = \frac{1}{\beta}\ln t + \frac{1}{\beta}\ln(\alpha\beta) \quad (6)$$

where α is the initial adsorption rate (mg/(g min)) and β is the desorption rate (mg/g).

The intra-particle diffusion was explored using a linear intra-particle diffusion kinetic model, which can be expressed by Eq. (7):

$$q_t = K_p t^{1/2} + C \quad (7)$$

where K_p is the intra-particle diffusion rate constant (mg/(g min$^{1/2}$)) and C is a constant related to the thickness of the boundary layer (mg/g).

If the plot of q_t vs. $t^{1/2}$ gives a straight line, the sorption process is controlled by intra-particle diffusion only.

2.3.4. Adsorption isotherm models

2.3.4.1. Langmuir isotherm

The Langmuir isotherm is most widely used for the sorption of a pollutant from a liquid solution. The model assumes that the sorption takes place at specific homogenous sites within the adsorbent. The Langmuir equation is represented as follows:

$$q_e = \frac{q_0 K_L C_e}{(1 + K_L C_e)} \quad (8)$$

where q_e is the mass of phosphate ions adsorbed on the adsorbent at equilibrium (mg/g), C_e is the equilibrium concentration of phosphate ions (mg/L), q_0 is the maximum adsorption capacity (mg/g), and K_L is a Langmuir constant (L/mg) related to the energy of adsorption.

The linear form of the Langmuir isotherm is:

$$\frac{C_e}{q_e} = \frac{C_e}{q_0} + \frac{1}{K_L q_0} \quad (9)$$

The essential characteristic of the Langmuir isotherm may be expressed in terms of a dimensionless separation parameter R_L, which is indicative of the isotherm shape that predicts whether an adsorption system is unfavourable ($R_L > 1$), linear ($R_L = 1$), or favourable ($0 < R_L$). R_L is defined as:

$$R_L = \frac{1}{(1 + (1 + K_L / C_0))} \quad (10)$$

where C_0 is the initial concentration (mg/L).

2.3.4.2. Freundlich isotherm

The Freundlich isotherm is an empirical equation to describe heterogeneous adsorption systems. This isotherm is given as:

$$q_e = K_F C_e^{1/n} \quad (11)$$

where K_F is the Freundlich constant (L/g) related to the bonding energy and $1/n$ is the heterogeneity factor in which n is a measure of the deviation from linearity of the adsorption. A linear form of the Freundlich expression is:

$$\log q_e = \log K_F + \frac{1}{n}\log C_e \quad (12)$$

2.3.4.3. Temkin isotherm

The Temkin isotherm has been used in the following form:

$$q_e = \frac{RT}{b}\ln(K_T C_e) \quad (13)$$

where $RT/b = B$, R is the gas constant (8.31 J/Mol K), T is the absolute temperature, K_T is the Temkin isotherm equilibrium binding constant (L/g), and b is the Temkin isotherm constant.

A linear form of the Temkin isotherm can be expressed as:

$$q_e = \frac{RT}{b}\ln(K_T) + \frac{RT}{b}\ln(C_e) \quad (14)$$

2.3.4.4. Dubinin–Radushkevich isotherm

The Dubinin–Radushkevich isotherm assumes that there is a surface area where the adsorption energy is homogeneous. The Dubinin–Radushkevich equation has the following form:

$$q_e = q_{\max}(\mathrm{Exp})^{-K_D^2} \quad (15)$$

where $q_{\max}$ is the Dubinin–Radushkevich monolayer capacity (mg/g), K_D is the constant related to the mean free energy (E) of adsorption per mole of the adsorbate (mol^2/kJ^2), which can be computed using the relationship:

$$E = (2k)^{-1/2} \quad (16)$$

and ε is the Polanyi potential, which is related to the equilibrium concentration as follows:

$$\varepsilon = RT\ln\left(1 + \frac{1}{C_e}\right) \quad (17)$$

A linear form of the Dubinin–Radushkevich isotherm is:

$$\ln q_e = \ln q_{\max} - k_D \varepsilon^2 \quad (18)$$

In this analysis, the correlation coefficient (r^2) and nonlinear chi-square test (χ^2) were used to determine the best-fitting

isotherm with the experimental data. The mathematical derivation is given by Eq. (19).

$$\chi^2 = \sum \left(\frac{\left(q_e - q_{e,\text{cal}}\right)^2}{q_e} \right) \tag{19}$$

where $q_{e,\text{cal}}$ is the equilibrium capacity (mg/g) calculated from the model.

χ^2 will be a small number when the data from the model are similar to the experimental data.

3. Results and discussion

3.1. Characterisation of A. mauritanicus stem-derived activated carbon

The AMSAC prepared under the condition mentioned above was produced with a final yield of 37.54 wt.%, which is a similar value to those reported previously by other authors [23–25]. In view of the data in Table 1, AMSAC shows a high moisture content (9.63%), low percentage of volatile matter (30.5%), average bulk density (0.255 g/mL), high fixed carbon content (54.15%), and low ash content (6.72%). Furthermore, the impregnation of stems with H_3PO_4 followed by a thermal treatment under nitrogen gas creates cavities on the surface of the activated carbon and increases its porosity and specific surface area due to the evaporation of activating agents during carbonization [26,27]. The BET surface area results indicate that AMSAC has a surface area of 1,293 m^2/g. This value is higher than that reported by Lim et al. [28], who reported a surface area of 1,109 m^2/g from palm shells. Also, the surface area in this study is higher than that reported by Liu et al. [29], who prepared activated carbon with a surface area of 1,179 m^2/g from lotus stalks by H_3PO_4 activation. The prepared activated carbon in this study has a pore surface area, pore diameter, pore volume, and miro-pore volume of 165.7 m^2/g, 1.93 nm, 1.23 m^3/g, and 1.17 m^3/g, respectively. In addition, the iodine adsorption number (1,043 mg/g) and methylene blue adsorption number (427 mg/g) measurements showed that the AMSAC was able to absorb small and large molecules equally well, suggesting the existence of a highly microporous structure.

The SEM images in Fig. 2 show the surface morphologies of AMSAC under two magnifications, 77x and 1,138x. It can be seen that AMSAC has an irregular fully solid structure with porous cavities distributed on its surface. The formation of the porous structure can result from evaporation and breakdown of the non-carbon compounds contained in the stem of the *A. mauritanicus*. Large and well-developed pores were clearly found on the surface of the activated carbon. The presence of the activator can enlarge the pores of activated carbon and expand its surface [30,31].

Fig. 3 shows the XRD pattern of the AMSAC sample. This activated carbon, which exhibits broad diffraction peaks and the absence of a sharp peak, reveals a predominantly amorphous structure [30,32]. There are two centered broad diffraction peaks around 2θ = 23° and 44° in the spectrum,

Table 1
Characterisation of AMSAC prepared by phosphoric acid

Parameter	Value
Bulk density (g/mL)	0.255
Ash content (%)	6.72
Moisture (%)	9.63
Volatile matter (%)	30.5
Yield (%)	37.54
Iodine number (mg/g)	1,043
Methylene blue number (mg/g)	427
S_{BET} (m^2/g)	1,293
Pore specific surface (m^2/g)	165.7
Total pore specific volume (cm^3/g)	1.23
Micropore volume (cm^3/g)	1.17
Average pore diameter (nm)	1.93

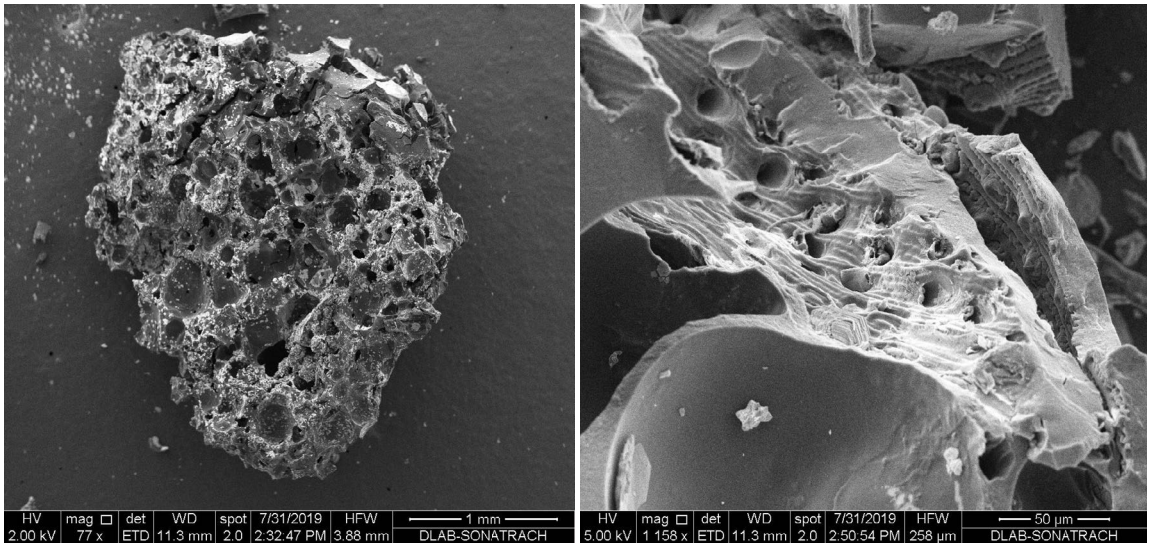

Fig. 2. SEM micrographs of AMSAC (*A* = 77x and *B* = 1,138x).

corresponding to the diffraction of (002) and (100), respectively. The appearance of the peak at around 23° at an activation temperature of 500°C signifies an increasing regularity of the crystalline structure, which will result in a better layer alignment [33]. The crystallinity recorded by AMSAC is 7.2% with 92.8% amorphous. These results were close to previous studies that used different lignocellulosic raw materials [33–35].

The FTIR spectrum of AMSAC (Fig. 4) shows an absorption band at 3,700–3,100 cm^{-1}, with a maximum at about 3,400–3,340 cm^{-1}, which is characteristic of the stretching vibration of the hydrogen-bonded hydroxyl of phenolic

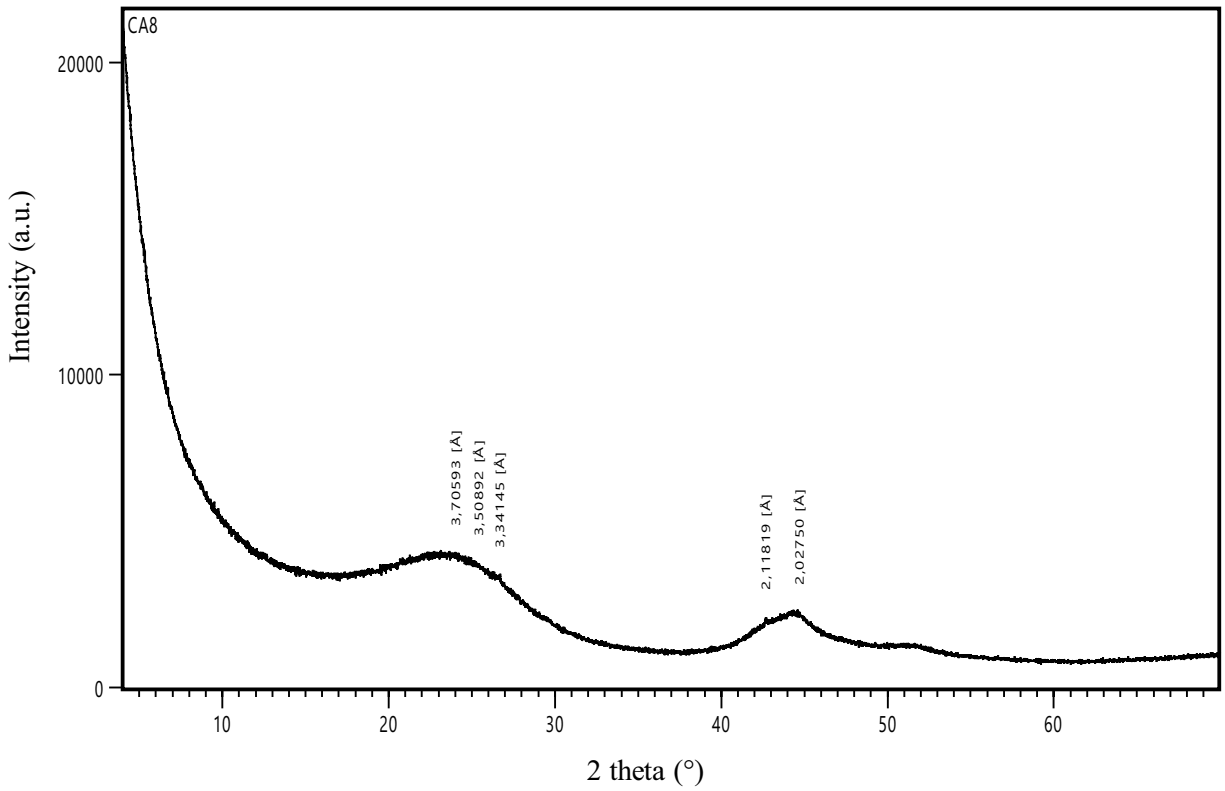

Fig. 3. X-ray diffraction pattern of the AMSAC sample.

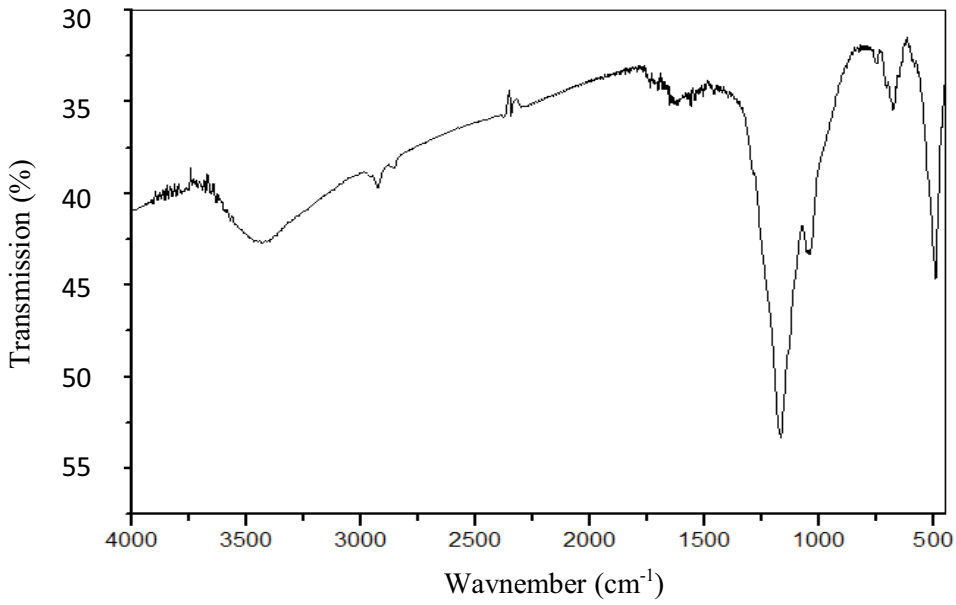

Fig. 4. FTIR spectrum of AMSAC.

groups [36]. The band at 2,800–3,000 cm^{-1} indicates the presence of an aliphatic C–H. The spectrum shows a small peak at 1,695–1,710 cm^{-1}, according to Montes-Morán et al. [37], that can be assigned to the C=C symmetrical stretching of pyrone groups and C=O of carboxylic groups. The band at 1,000–1,300 cm^{-1} is usually found with oxidized carbons and has been assigned to C–O stretching in acids, alcohols, phenols, ethers, and/or esters groups [38]. In addition, the vibration bands located at 1,026 cm^{-1} can be ascribed to the stretching modes of Si–O–Si, representing the existence of silicate functional groups. Furthermore, the peaks at 680–700 cm^{-1} are an indication of Si–Si bonds [39].

3.2. Effect of time

Fig. 5 shows the results obtained from adsorption kinetics experiments with AMSAC. According to this plot, the PO_4^{-3} removal was characterized by a fast increase in PO_4^{-3} adsorption in the first 4 min of contact. This fast increase was due to the availability of a large number of vacant sites for adsorption during the initial stages. With the occurrence of the reaction, the number of active sites on the AMSAC decreases continuously, and the concentration gradient diminishes, finally reaching equilibrium. The equilibrium for phosphate ion adsorption onto the AMSAC was reached in approximately 45 min, with the maximum uptake removal of 4.5 mg/g. The data shown in Fig. 5 were used to determine kinetic parameters in the kinetic models tested.

3.3. Effect of initial phosphate ion concentration

The effect of initial PO_4^{-3} concentrations between 10 and 60 mg/L in the solutions on the rate of adsorption onto AMSAC was investigated. As shown in Fig. 6, with an increase in PO_4^{-3} concentration, the removal efficiency decreases from 84.43% at 10 mg PO_4^{-3}/L to 61.68% for the extreme concentration of 60 mg PO_4^{-3}/L with the same contact time, initial pH, and adsorption temperature. Generally, there are several adsorption steps involved in the transfer of a solute in adsorption dynamics: film diffusion, particle diffusion, and the interior surface sorption. An increase in the uptake rate to the maximum adsorption capacities was observed at lower concentrations of PO_4^{-3} ions, which demonstrated that the uptake of phosphate ions by the AMSAC surface was very fast (Fig. 6).

3.4. Effect of initial potential hydrogen

The dissociation constants pK_1, pK_2, and pK_3 of H_3PO_4 are 2.15, 7.20, and 12.33, respectively. Depending on the pH of the solution, PO_4^{-3} exists as H_3PO_4, HPO_4^{-1}, HPO_4^{-2}, and PO_4^{-3}. So, the adsorption of phosphate depends on the pH of the solution. Therefore, it is necessary to consider the different ionic species of phosphate when investigating the adsorption reaction. Fig. 7 shows the effect of initial pH on the removal of PO_4^{-3} by AMSAC. For pH < 6 and pH > 10, the removal is lower, and for 6 < pH < 10, the removal of PO_4^{-3} is higher and reaches a maximum percent of around 75% at pH = 6–7. A similar type of behavior has also been reported for the adsorption of phosphate ions from an aqueous solution on activated carbon [40,41]. At pH = 2, the PO_4^{-2} exists predominantly as H_3PO_4, which is weakly attached to the sites of the adsorbent [42]. For 6 < pH < 10, prevalent species of PO_4^{-3}, such as $H_2PO_4^{-1}$ and HPO_4^{-2}, are anionic in nature and are easily adsorbed onto the positive surface of the adsorbent. The low phosphate uptake for pH > 10 can be attributed to the competition of hydroxide ions with phosphate ions for adsorption sites. Furthermore, the negatively charged phosphate ions at high pH can also be attributed to electrostatic repulsion with the negatively charged AMSAC surface.

3.5. Adsorption kinetic

Kinetic studies are generally used to describe the rate and extent of the adsorption of the adsorbate onto the adsorbent and to control the residual time of the whole

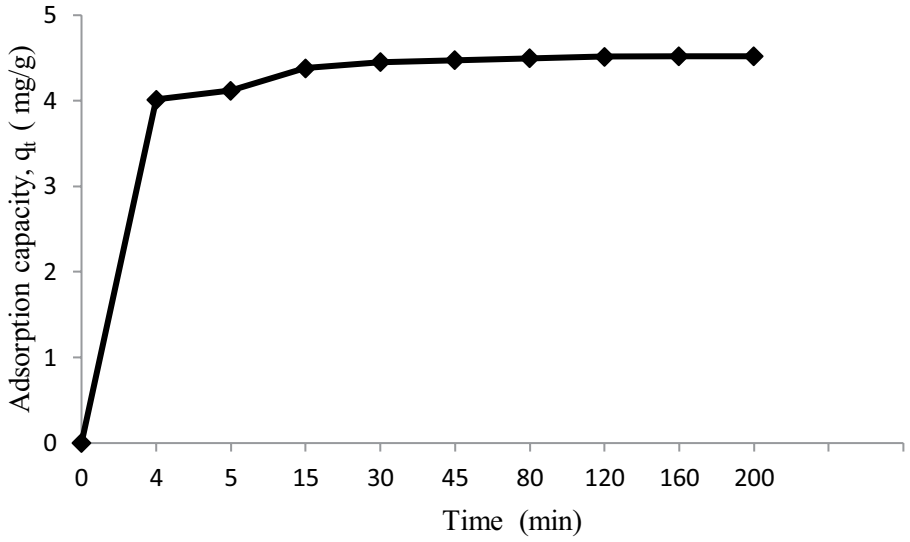

Fig. 5. Effect of contact time on phosphate removal by AMSAC (temperature: 25°C; pH = 6.5; phosphate concentration: 40 mg/L; adsorbent concentration: 4 g/L).

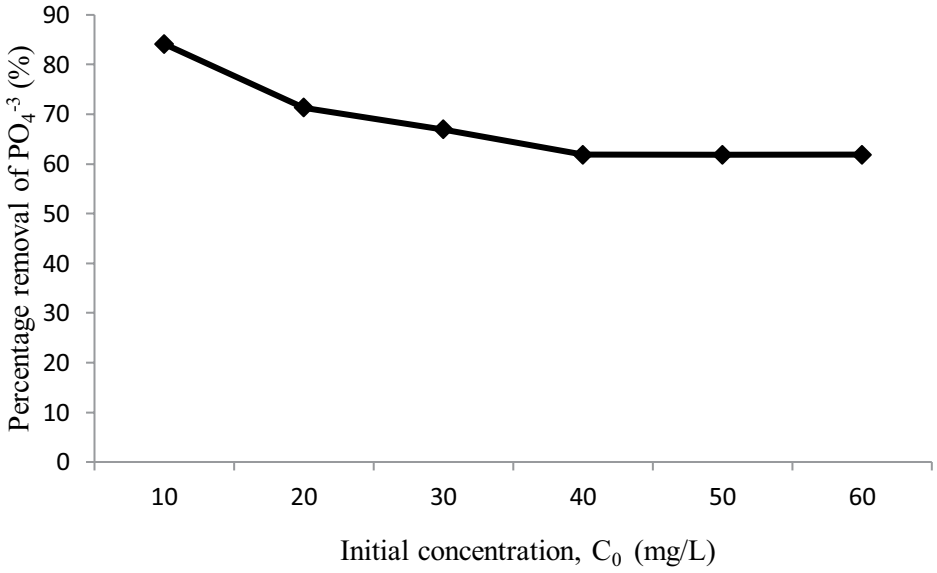

Fig. 6. Effect of initial phosphate ion concentration on the rate of adsorption (pH = 6.5; T = 25°C; t = 45 min; 4 g/L adsorbent).

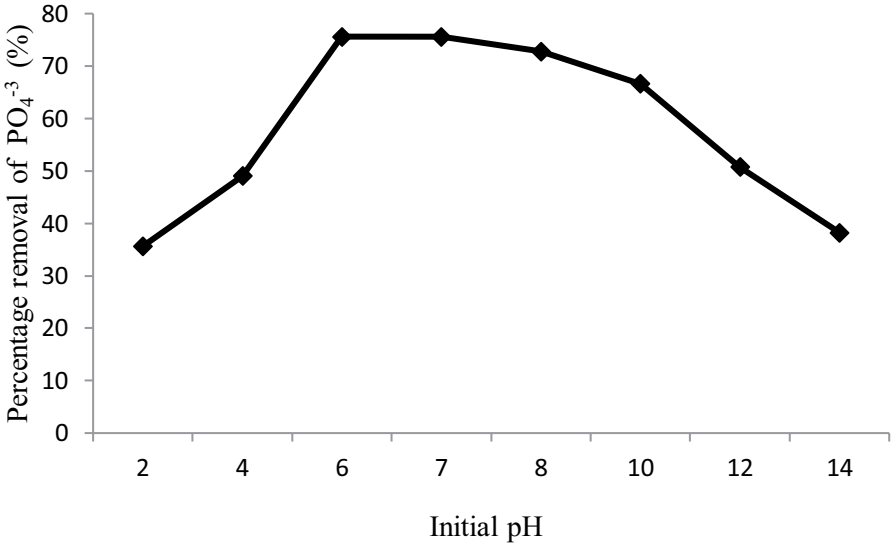

Fig. 7. Effect of initial pH on the adsorption of phosphate ions, T = 25°C ± 1°C; t = 200 min; C_0 = 40 mg/L; adsorbent dose = 4 g/L.

adsorption process. Hence, the adsorption rate constant values for PO_4^{-3} adsorption onto AMSAC were determined by curve fitting, with results as shown in Figs. 8–11. The constants are reported in Table 2. It can be seen that the experimental data fit better with the pseudo-second-order model, with a determination coefficient (R^2) of 0.998, compared with the first-order model, with an R^2 of 0.938. In addition, the equilibrium sorption capacities (q_e) calculated by the pseudo-second-order model were closer to the experimental values, and the Chi-square test was also carried out to support the best fitting adsorption model. Similar results have been reported for the adsorption of PO_4^{-3} onto Leftover coal [43], commercial activated carbon [44], peat-based biosorbent [45], biosorbent lignocellulosic butanol residue [46], and peat [40]. On the other hand, the initial adsorption rate α and coefficient β of activated energy of the Elovich model, as shown in Table 2, implies that the Elovich model is not suitable to describe the adsorption process compared with the other models mentioned above. In terms of the intra-particle diffusion model, it can be seen that the R^2 was 0.648 for the whole adsorption process, while it was 0.974 for the initial time of the adsorption process, which indicates that the intra-particle diffusion is the limiting step at the initial time of the adsorption process [47,48].

3.6. Adsorption isotherm

The Langmuir, Freundlich, Temkin, and Dubinin–Radushkevich equations expressed in Eqs. (8), (11), (13), and (15) were used to evaluate these adsorption isotherm data. All available adsorption isotherm models are composed of certain constant values, which are assigned to specific surface

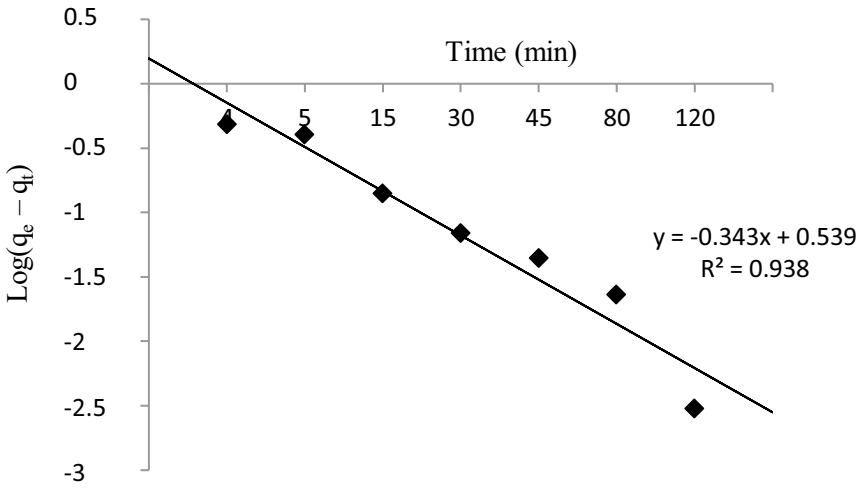

Fig. 8. Pseudo-first-order kinetic model of the adsorption of PO_4^{-3} onto AMSAC.

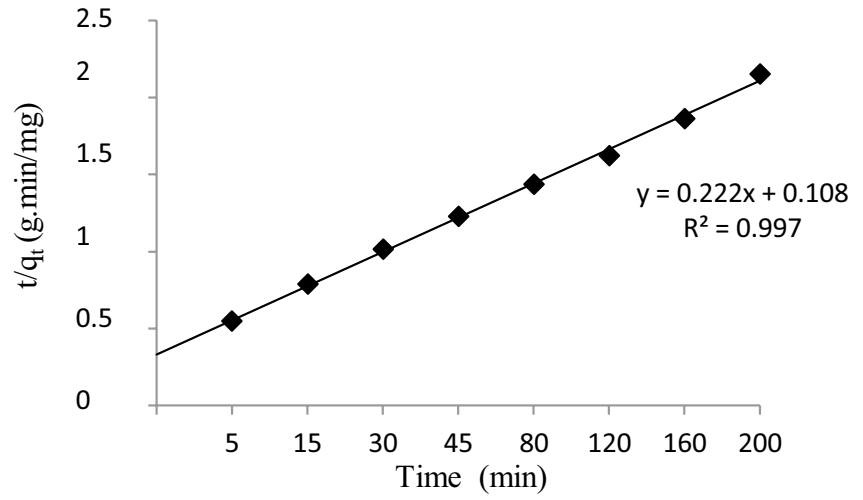

Fig. 9. Pseudo-second-order kinetic model of the adsorption of PO_4^{-3} onto AMSAC.

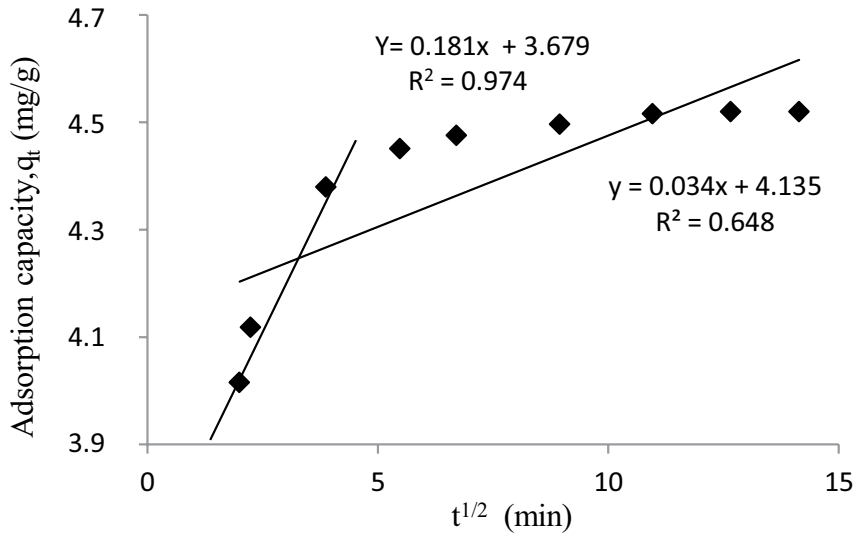

Fig. 10. Intraparticular kinetic model adsorption of PO_4^{-3} onto AMSAC.

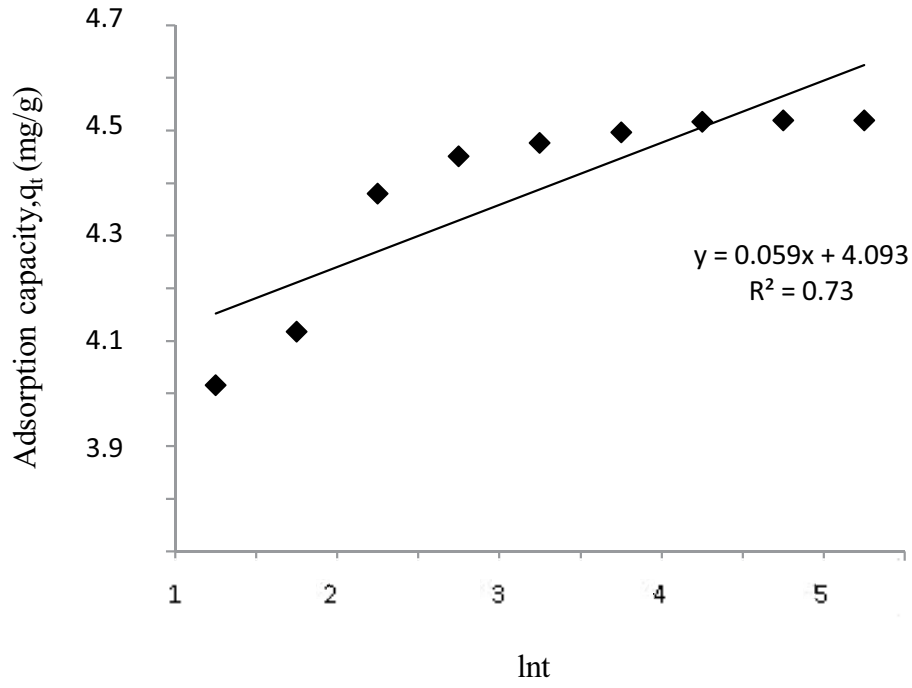

Fig. 11. Elovich kinetic model of the adsorption of PO_4^{-3} onto AMSAC.

Table 2
Kinetic parameters for removal of phosphate ions from an aqueous solution by AMSAC (pH = 6.8, T = 25°C ± 1°C, C_0 = 40 ml/L, and AMSAC dose = 4 g/L)

Kinetic model	Equation	Parameter	Value	x_t^2
Pseudo-first-order	$\log(q_e - q_t) = \log(q_e) - (K_1/2.303)\cdot t$	R^2	0.938	0.015878
		q_e (mg/g)	3.46	
		K_1 (min)	0.789	
Pseudo-second-order	$t/q_t = (1/K_2 q_e^2) + (1/q_e)t$	R^2	0.997	0.000348
		q_e (mg/g)	4.5	
		K_2 (g/mg min)	0.049	
Simple Elovich	$q_t = 1/\beta \ln(\alpha\beta) + 1/\beta \ln t$	R^2	0.73	0.0167
		α (mg/g min)	7.956×10^{28}	
		β (g/mg)	16.95	
Intra-particle diffusion	$q_t = K_p t^{1/2} + C$	R^2	0.648	0.0134
		C	4.135	
		K_p (mg/g $min^{-1/2}$)	0.034	

behavior and used to compare the adsorption properties of the adsorbents against adsorbates [49]. The interaction of phosphate ions in the liquid phase and the AMSAC solid phase was described by Freundlich, Langmuir, Temkin, and Dubinin–Radushkevich isotherm models. The plots are presented in Figs. 12–15, and the relative parameters are listed in Table 3. It can be seen that all the isotherms showed a similar shape and were nonlinear over a wide range of aqueous equilibrium concentrations. It was observed from Table 3 that the Langmuir fitting plot with a determination coefficient of R^2 = 0.976 and nonlinear Chi-square test of χ^2 = 0.225 fit the experimental data better than the Freundlich, Temkin, and Dubinin–Radushkevich isotherms. Since the Langmuir model is more suitable to describe the experimental data, this suggests that the sorbent surface has uniformly distributed homogenous surface adsorption sites available for the adsorbate ions. It also assumes that, during adsorption, the energy is uniformly distributed between the adsorbate surface and adsorbent molecules for monolayer adsorption regardless of the pH and the temperature effect [50]. The theoretical complete monolayer coverage of PO_4^{-3} on AMSAC was calculated to be 4.17 mg/g compared to the experimentally determined value of 4.52 mg/g, and K_L (Langmuir isotherm constant) was 1.498 L/mg. The sorption capacity of the AMSAC obtained in this study can be regarded as relatively high and could be compared to other materials

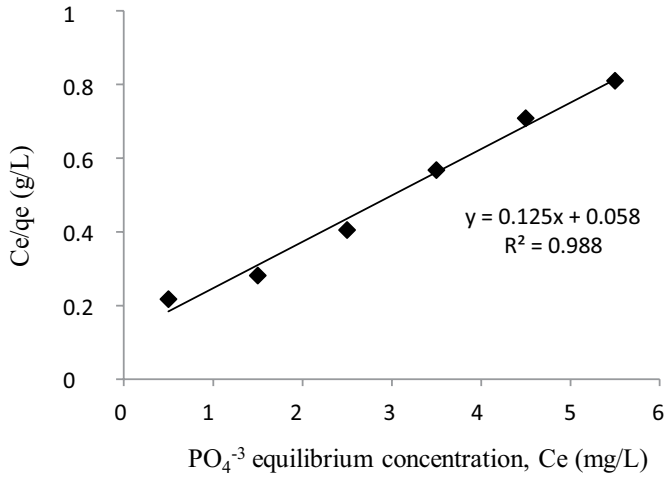

Fig. 12. Langmuir plot of adsorption for PO_4^{-3} onto AMSAC.

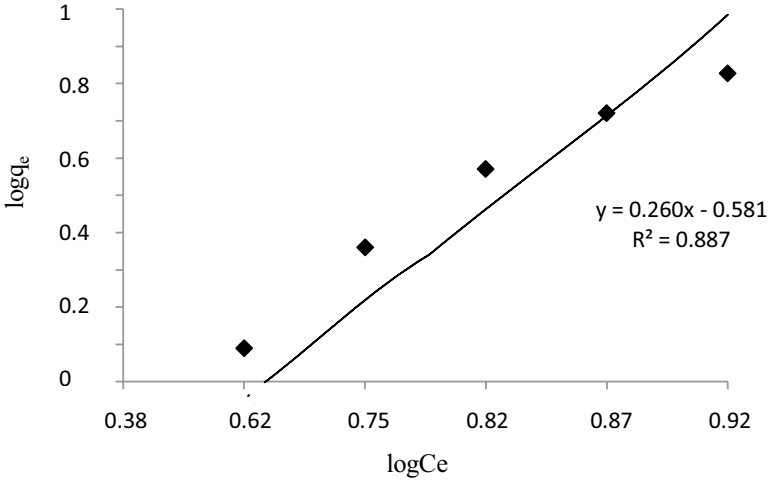

Fig. 13. Freundlich plot for adsorption of PO_4^{-3} onto AMSAC.

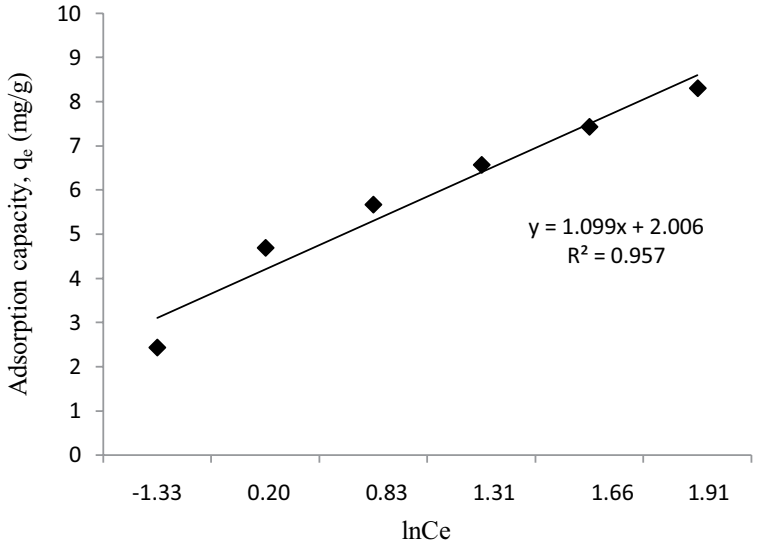

Fig. 14. Temkin plot for adsorption of PO_4^{-3} onto AMSAC.

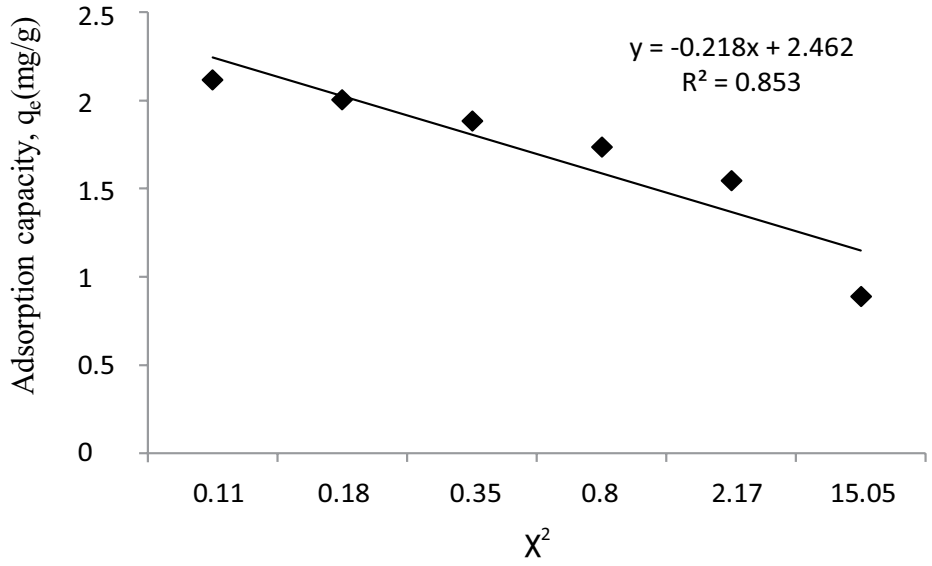

Fig. 15. Dubinin–Radushkevich plot for adsorption of PO_4^{-3} onto AMSAC.

Table 3
Isotherm constant for the adsorption of phosphate ions onto AMSAC

Isotherm	Equation	Parameter	Value	X_t^2
Langmiur	$C_e/q_e = 1/(K_L q_{max}) + C_e/q_{max}$	R^2	0.976	0.225
	$R_L = 1/(1 + K_L C_0)$	q_{max} (mg/g)	4.17	
		K_L (L/mg)	1.498	
		R_L	0.143	
Freundlich	$\log q_e = \log K_F + (1/n)\log C_e$	R^2	0.870	5.148
		K_f (L/mg)	4.246	
		n	9.708	
Temkin	$q_e = B\ln(k_T) + B\ln(C_e)$	R^2	0.953	1.218
	$B = RT/b$	K_T (L/mg)	4.284	
		B (J/mol)	2.137	
		b	1,158.81	
Dubinin–Radushkevich	$\ln q_e = \ln q_{max} - k_D\varepsilon^2$	R^2	0.87	9.116
	$\varepsilon = RT\ln(1 + 1/C_e)$	q_{max} (mg/g)	11.72	
	$E = (2k_D)^{-1/2}$	K_D (mol²/kJ²)	0.218	
		E (kJ/mol)	0.748	

reported in the literature (Table 4). Also, according to the data presented in Table 3, the favorable Langmuir isotherm is observed for R_L (the separation factor) values greater than 0 and lesser than 1. The low value of R_L = 0.143 indicates high and favorable adsorption of PO_4^{-3} onto AMSAC [60].

4. Conclusion

Microporous activated carbons with a significant contribution of mesoporosity were obtained by H_3PO_4 activation of *A. mauritanicus* stems. Activated carbon developed a surface area of 1,292 m²/g and a pore volume of 1.23 cm²/g. The XRD, BET, and FTIR techniques confirmed the successful elimination of the major mineral fraction on the AC samples. In batch mode studies, the phosphate ion removal by AMSAC was influenced by solution pH, initial concentration, and contact time. At pH = 7, AMSAC can remove around 75% PO_4^{-3} from the solution with an initial phosphate ion concentration of 40 mg/L and a temperature of 25°C. Among the models applied to fit the adsorption kinetic data, the pseudo-second-order rate equation allowed for a better reproduction of the experimental results. It is also worth noting that the application of the intra-particle diffusion model showed that this phenomenon is the only rate-controlling step during the first stage of batch-wise adsorption, which extended upto around 30 min when most of the PO_4^{-3} uptake takes place. The Langmuir isotherm model fit the experimental equilibrium data well, indicating the homogeneity of the adsorptive sites on the AMSAC particle surface and monolayer adsorption. However, to compete with

Table 4
Comparison of maximum adsorption capacity of phosphate by different adsorbents

Adsorbent	q_m (mg/g)	Reference
Red mud	0.58	[51]
Peat	8.91	[40]
Al-bentonite	5.05	[52]
Na-natural zeolite	2.19	[53]
Steel furnace slag	1.43	[54]
Fly ash	20.16	[55]
Iron oxide tailings	8.21	[56]
Iron-modified peat	11.53	[45]
Different kinds of sand	0.29	[57]
Mineral apatite	~0.3	[58]
Goethite	6.42	[59]
Activated coir pith carbon	7.262	[42]
This study	4.52	

other adsorbents, some modifications need to be made to enhance the efficiency of the AMSAC to remove phosphate ions. These modifications will be performed in future works.

Acknowledgement

The authors wish to thank M'Hamed Bougara University and the research center of SONATRACH at Boumerdes for their technical support during the course of work.

Symbols

S_{BET}	—	The specific surface area calculated via BET equation, m^2/g
q_m	—	Maximum adsorption capacity, mg/g
q_e	—	Adsorption capacity at equilibrium, mg/g
q_{cal}	—	Calculated amount, mg/g
q_t	—	Adsorption capacity at time t, mg/g
B	—	Temkin isotherm energy of adsorption, J/mol
b	—	Temkin isotherm constant
K_T	—	Temkin isotherm equilibrium binding constant, L/g
C_0	—	Initial concentration of adsorbate, mg/L
C_e	—	Equilibrium concentration of adsorbate, mg/L
K_L	—	Langmuir isotherm constant, L/mg
K_1	—	Constant pseudo-first-order model
K_2	—	Constant pseudo-second-order model
K_p	—	Intra-particle diffusion rate constant, mg/(g $min^{1/2}$)
C	—	Constant related to the thickness of the boundary layer, mg/g.
α	—	Initial adsorption rate, mg/(g min)
β	—	Desorption rate, mg/g
K_F, n	—	Freundlich isotherm constants, mg/g
R_L	—	Separation parameter
ε	—	Polanyi potential
χ^2	—	Chi-square test
R^2	—	Correlation coefficient
K_D	—	Dubinin–Radushkevich constant, mol^2/kJ^2
E	—	Free energy, kJ/mol
R	—	Universal gas constant, 8.314 J/mol K
T	—	Temperature, °C

References

[1] S. Tanada, M. Kabayama, N. Kawasaki, T. Sakiyama, T. Nakamura, M. Araki, T. Tamura, Removal of phosphate by aluminum oxide hydroxide, J. Colloid Interface Sci., 257 (2003) 135–140.
[2] P.U.Verma, A.R. Purohit, N.J. Patel, Pollution status of Chandlodia Lake located in Ahmedabad Gujarat, Int. J. Eng. Res. Appl., 2 (2012) 1600–1610.
[3] D. Yadav, M. Kapur, P. Kumar, M. K. Mondal, Adsorptive removal of phosphate from aqueous solution using rice husk and fruit juice residue, Process Saf. Environ. Prot., 94 (2015) 402–409.
[4] M. Arshadi, H. Eskandarloo, M. Azizi, A. Abbaspourrad, M.K. Abdolmaleki, H. Eskandarloo, A. pourrad, Synthesis of highly monodispersed, stable, and spherical NZVI of 20–30 Nm on filter paper for the removal of phosphate from wastewater: batch and column study, ACS Sustainable Chem. Eng., 6 (2018) 11662–11676.
[5] E.N. Peleka, E.A. Deliyanni, Adsorptive removal of phosphates from aqueous solutions, Desalination, 245 (2009) 357–371.
[6] L. Chen, X. Zhao, B. Pan, W. Zhang, M. Hua, L. Lv, W. Zhang, Preferable removal of phosphate from water sing hydrous zirconium oxide-based nanocomposite of high stability, J. Hazard. Mater., 284 (2015) 35–42.
[7] S. Yeoman, T. Stephenson, J.N. Lester, R. Perry, The removal of phosphorus during wastewater treatment: a review, Environ. Pollut., 49 (1998) 183–233.
[8] A.N. Shilton, I. Elmetri, A. Drizo, S. Pratt, R.G. Haverkamp, S.C. Bilby, Phosphorus removal by an "active" slag filter-a decade of full scale experience, Water Res., 40 (2006) 113–118.
[9] Y. Zhang, R. Gao, M. Liu, C. Yan, A. Shan, Adsorption of modified halloysite nanotubes in vitro and the protective effect in rats exposed to zearalenone, Arch. Anim. Nutr., 68 (2014) 320–335.
[10] A. Bhatnagar, M. Sillanpää, A review of emerging adsorbents for nitrate removal from water, Chem. Eng. J., 168 (2011) 493–504.
[11] F.J. Zhang, H.Y. Zhang, L.Y. Zhang, The removal of phosphate by Coal Gangue from wastewater, Appl. Mech. Mater., 209 (2012) 2005–2008.
[12] Y. Yao, B. Gao, M. Inyang, Biochar derived from anaerobically digested sugar beet tailings: characterization and phosphate removal potential, Bioresour. Technol., 102 (2011) 6273–6278.
[13] F. Faraoun, M.A. Bouzidi, I. Attaoui, A. Latreche, H. Meliani, M. Benyahia, Caractérisation des formations végétales à Ampelodesmos mauritanicus sur Djebel Tessala, Algérie occidentale, Afrique Science, 12 (2016) 326–335.
[14] H. Zerganea, S. Abdia, H. Xub, J. Hemming, X. Wang, S. Willför, Y. Habibid, *Ampelodesmos mauritanicus* a new sustainable source for nanocellulose substrates, Ind. Crops Prod., 144 (2020) 112044, doi: 10.1016/j.indcrop.2019.112044.
[15] F. Luzia, D. Pugliaa, F. Sarasinib, J. Tirillòb, G. Maffeib, A. Zuorrob, R. Lavecchiab, J.M. Kennya, L. Torrea, Valorization and extraction of cellulose nanocrystals from North African Grass: *Ampelodesmos mauritanicus* (Diss.), Carbohydr. Polym., 209 (2019) 328–337.
[16] M.E.H. Bourahli, H. Osmani, Chemical and mechanical properties of diss (*Ampelodesmos mauritanicus*) fibers, J. Nat. Fibers, 10 (2013) 219–232.
[17] L. Yu, Y.M. Luo, Fabrication, characterization and evaluation of mesoporous activated carbons from an agricultural waste: Jerusalem artichoke stalk as an example, Front. Environ. Sci. Eng., 9 (2013) 206–215.
[18] S. Toshiguki, K. Yukata, Pyrolysis of plant, animal and human wastes; physical and chemical characterization of the pyrolytic product, Bioresour. Technol., 90 (2003) 241–247.

[19] I. Langmuir, The adsorption of gases on plane surfaces of glass, mica and platinum, J. Am. Chem. Soc., 40 (1918) 1362–1403.
[20] ASTM, Standard Test Method for Total Ash Content of Activated Carbon (ASTM-D2866-94), American Society for Testing and Materials, Philadelphia, 1995.
[21] B. Bestani, N. Benderdouche, B. Bensttali, B. Mostefa, A. Addou, Methylene blue and iodine adsorption onto an activated desert plant, Bioresour. Technol., 99 (2008) 8441–8444.
[22] M. Rafatullah, O. Sulaiman, R. Hachim, A. Ahmed, Adsorption of methylene blue on low-cost adsorbents: a review, J. Hazard. Mater., 177 (2010) 70–80.
[23] I. EL Aboudia, H. Annaba, A. Mdarhria, M. Amjouda, L. Servantc, Activated carbon synthesis using Moroccan dates stones as precursor and application for wastewater treatment, J. Mater. Environ. Sci., 8 (2017) 1483–1481.
[24] M.A. Nahil, P.T. Wiliams, Pore characteristics of activated carbons from the phosphoric acid chemical activation of cotton stalks, Biomass Bioenergy, 37 (2012) 142–149.
[25] J. Guo, A.C. Lua, Textural and chemical properties of adsorbent prepared from palm shell by phosphoric acid activation, Mater. Chem. Phys., 80 (2003) 114–119.
[26] B. Hong, G. Xue, L. Weng, X. Guo, Pretreatment of moso bamboo with dilute phosphoric acid, BioResources, 7 (2012) 4902–4913.
[27] S.S. Thanapal, W. Chen, K. Annamalai, N. Carlin, R.J. Ansley, D. Ranjan, Carbon dioxide torrefaction of woody biomass, Energy Fuels, 28 (2014) 1147–1157.
[28] W.C. Lim, C. Srinivasakannan, N. Balasubramanian, Activation of palm shells by phosphoric acid impregnation for high yielding activated carbon, J. Anal. Appl. Pyrolysis, 88 (2010) 181–186.
[29] H. Liu, J. Zhang, C. Zhang, N. Bao, C. Cheng, Activated carbons with well-developed microporosity and high surface acidity prepared from lotus stalks by organophosphorus compounds activations, Carbon, 60 (2013) 289–291.
[30] M. Jagtoyen, F. Derbyshire, Activated carbons from yellow poplar and white oak by H_3PO_4 activation, Carbon, 36 (1998) 1085–1094.
[31] K. Schrodter, G. Bettermann, T. Staffel, T. Hofman, Ullmann's Encyclopedia of Industrial Chemistry, Vol. A19, VCH, Weinheim, 1991.
[32] M.S. Shamsuddina, N.R.N. Yusoffa, M.A. Sulaimana, Synthesis and characterization of activated carbon produced from kenaf core fiber using H_3PO_4 activation, Procedia Chem., 19 (2016) 558–565.
[33] P. Barpanda, G. Fanchini, G.G. Amatucci, Structure, surface morphology and electrochemical properties of brominated activated carbons, Carbon, 49 (2011) 2538–2548.
[34] J. Xu, L. Chen, H. Qu, Y. Jiao, J. Xie, G. Xing, Preparation and characterization of activated carbon from reedy grass leaves by chemical activation with H_3PO_4 Jianzhong, Appl. Surf. Sci., 320 (2014) 674–680.
[35] A.A. Babar, I. Panhwar, S. Qureshi, S. Memon, Z. Siddiqui, Utilization of biomass rice straw to produce activated charcoal through single stage pyrolysis process, J. Int. Environ., 14 (2019) 1–6.
[36] V.G. Serrano, J.P. Villegas, A.P. Florindo, C.D. Valle, C.V. Calahorro, FT-IR study of rockrose and of char and activated carbon, J. Anal. Appl. Pyrolysis, 36 (1996) 71–80.
[37] M.A. Montes-Moran, D. Suarez, J.A. Menendez, E. Fuente, On the nature of basic sites on carbon surfaces: an overview, Carbon, 42 (2004) 1219–1225.
[38] J.L. Figueiredo, M.F.R. Pereira, M.M.A. Freitas, J.J.M. Órfão, Modefication of the surface chemistry of activated carbones, Carbon, 37 (1999) 1379–1389.
[39] J. Zou, Y. Dai, X. Wang, Z. Ren, C. Tian, K. Pan, S. Li, M. Abuobeidah, H. Fu, Structure and adsorption properties of sewage sludge-derived carbon with removal of inorganic impurities and high porosity, Bioresour. Technol., 142 (2013) 209–217.
[40] J.B. Xiong, Q. Mahmood, Adsorptive removal of phosphate from aqueous media by peat, Desalination, 259 (2010) 59–64.
[41] X. Song, Y. Pan, Q. Wu, Z. Cheng, W. Ma, Phosphate removal from aqueous solutions by adsorption using ferric sludge, Desalination, 280 (2011) 384–390.
[42] P. Kumar, S. Sudha, S. Chand, V.C. Srivastava, Phosphate removal from aqueous solution using coir-pith activated carbon, Sep. Sci. Technol., 45 (2018) 1–8.
[43] D.T. Mekonnen, E. Alemayehu, B. Lennartz, Removal of phosphate ions from aqueous solutions by adsorption onto leftover coal, Water, 12 (2020) 1381, doi: 10.3390/w12051381.
[44] N. Mehrabia, M. Soleimania, H. Sharififarda, M.M. Yeganeha, Optimization of phosphate removal from drinking water with activated carbon using response surface methodology (RSM), Desal. Water Treat., 57 (2015) 15613–15618.
[45] A. Robaldsa, L. Dreijaltea, O. Bikovensb, M. Klavins, A novel peat-based biosorbent for the removal of phosphate from synthetic and real wastewater and possible utilization of spent sorbent in land application, Desal. Water Treat., 57 (2016) 13285–13294.
[46] Z.X. Liu, J. Jiang, S. Fu, F.C. Zhejiang, Preparation and characterization of zirconia-loaded lignocellulosic butanol residue as a biosorbent for phosphate removal from aqueous solution, Appl. Surf. Sci., 387 (2016) 419–430.
[47] C.W. Cheung, J.F. Porter, G. McKay, Sorption kinetics for the removal of copper and zinc from effluents using bone char, Sep. Purif. Technol., 19 (2000) 55–64.
[48] M.A. Hanif, R. Naziya, M.N. Zafar, K. Akhtar, H.N. Bhatti, Kinetic studies for Ni(II) biosorption from industrial wastewater by *Cassia fistula* (Golden Shower) biomass, J. Hazard. Mater., 145 (2007) 501–505.
[49] M.C. Ncibi, Applicability of some statistical tools to predict optimum adsorption isotherm after linear and non-linear regression analysis, J. Hazard. Mater., 153 (2008) 207–212.
[50] M. Ghaedi, B. Sadeghian, A.A. Pebdani, R. Sahraei, A. Daneshfar, C. Duran, Kinetics, thermodynamics and equilibrium evaluation of direct yellow 12 removal by adsorption onto silver nanoparticles loaded activated carbon, Chem. Eng. J., 187 (2012) 133–141.
[51] W. Huang, S. Wang, Z. Zhu, L. Li, X. Yao, V. Rudolph, F. Haghseresht, Phosphate removal from wastewater using red mud, J. Hazard. Mater., 158 (2008) 35–42.
[52] L.G. Yan, Y.Y. Xu, H.Q. Yu, X.D. Xin, Q. Wei, B. Du, Adsorption of phosphate from aqueous solution by hydroxy-aluminum, hydroxy-iron and hydroxy-iron–aluminum pillared bentonites, J. Hazard. Mater., 179 (2010) 244–250.
[53] D. Wu, B. Zhang, C. Li, Z. Zhang, H. Kong, Simultaneous removal of ammonium and phosphate by zeolite synthesized from fly ash as influenced by salt treatment, J. Colloid Interface Sci., 304 (2006) 300–306.
[54] J. Xiong, Z. He, Q. Mahmood, D. Liu, Phosphate removal from solution using steel, slag through magnetic separation, J. Hazard. Mater., 152 (2008) 211–215.
[55] J. Chen, H. Kong, D. Wu, X. Chen, D. Zhang, Z. Sun, Phosphate immobilization from aqueous solution by fly ashes in relation to their composition, J. Hazard. Mater., 139 (2007) 293–300.
[56] L. Zeng, X. Li, J. Liu, Adsorptive removal of phosphate from aqueous solutions using iron oxide tailings, Water Res., 38 (2004) 1318–1326.
[57] D. Xu, J. Xu, J. Wu, A. Muhammad, Studies on the phosphorus sorption capacity of substrates used in constructed wetland systems, Chemosphere, 63 (2006) 344–352.
[58] N. Bellier, F. Chazarenc, Y. Comeau, Phosphorus removal from wastewater by mineral apatite, Water Res., 40 (2006) 2965–2971.
[59] O.K. Borggaard, B. Raben-Lange, A.L. Gimsing, B.W. Strobel, Influence of humic substances on phosphate adsorption by aluminium and iron oxides, Geoderma, 127 (2005) 270–279.
[60] T.W. Weber, R.K. Chakraborti, Pore and solid diffusion models for fixed bed adsorbents, AIChE J., 20 (1974) 228–238.